THE JOURNAL OF PHYSICAL CHEMISTRY B

Article

pubs.acs.org/JPCB

Competitive Binding of Cations to Duplex DNA Revealed through Molecular Dynamics Simulations

Jejoong Yoo[†,‡] and Aleksei Aksimentiev*[,†,‡,§]

[†]Department of Physics, University of Illinois at Urbana−Champaign, 1110 West Green Street, Urbana, Illinois 61801, United States

[‡]Center for the Physics of Living Cells

[§]Beckman Institute for Advanced Science and Technology

Supporting Information

ABSTRACT: The concept of "ion atmosphere" is prevalent in both theoretical and experimental studies of nucleic acid systems, yet the spatial arrangement and the composition of ions in the ion atmosphere remain elusive, in particular when several ionic species (e.g., Na^+, K^+, and Mg^{2+}) compete to neutralize the charge of a nucleic acid polyanion. Complementing the experimental study of Bai and co-workers (*J. Am. Chem. Soc.* **2007**, *129*, 14981), here we characterize ion atmosphere around double-stranded DNA through all-atom molecular dynamics simulations. We demonstrate that our improved parametrization of the all-atom model can quantitatively reproduce the experimental ion-count data. Our simulations determine the size of the ion atmosphere, the concentration profiles of ionic species competing to neutralize the DNA charge, and the sites of the cations' preferential binding at the surface of double-stranded DNA. We find that the effective size of the ion atmosphere depends on both the bulk concentration and valence of ions: increasing either reduces the size of the atmosphere. Near DNA, the concentration of Mg^{2+} is strongly enhanced compared to monovalent cations. Within the DNA grooves, the relative concentrations of cations depend on their bulk values. Nevertheless, the total charge of competing cations buried in the DNA grooves is constant and compensates for about ∼30% of the total DNA charge.

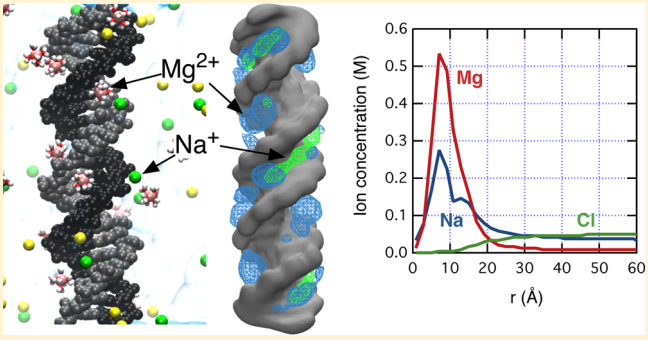

INTRODUCTION

The nucleic acids DNA and RNA are extraordinarily important biological macromolecules that encode the genetic blueprint of an entire living organism and carry instructions for protein synthesis.[1] Due to the polyanionic nature of nucleic acids, they are constantly surrounded by a condensed layer of counterions—the so-called "ion atmosphere", whose primary physical purpose is neutralization of the net charge of the nucleic acids.[2−4] Counterions are known to dramatically affect the structural stability and functional dynamics of nucleic acids. For instance, counterions can actively regulate packaging of genomes,[5,6] folding of RNA,[3,7,8] and ribozyme activity[9] and are essential mediators of DNA−protein interactions.[10] In the absence of counterions, electrostatic repulsion between nucleic acids is too strong to form the compact structures found in living organisms.[5,7]

Because physiological ionic solutions contain a mixture of various cations and anions of different size and charge (e.g., Na^+, K^+, Mg^{2+}, Ca^{2+}, and Cl^-), the ion atmosphere around nucleic acids consists of similar constituents. However, the concentration and spatial distribution of ions in the ion atmosphere are not necessarily the same as in the surrounding bulk solution.[4,11,12] Due to electrostatic attractions between cations and a nucleic acid, the charge density of condensed cations in the vicinity of the latter is comparable to the charge density of a nucleic acid (∼1 M),[11] independent of the cation density in the bulk. At the same time, a significant number of anions are excluded from the volume surrounding a nucleic acid due to electrostatic repulsion.[2,13] In the outer layer of the ion atmosphere—where ions are not in direct contact with the nucleic acid—the counterion motions are correlated because of their finite sizes and electrostatic repulsion.[11,14] In the inner layer of the ion atmosphere, cations also compete with one another for the same binding sites at the surface of nucleic acid.

In the case of double-stranded DNA (dsDNA), the interplay of short-range electrostatic attraction with the double-helical structure of the molecule creates conditions for selective binding of cations to the grooves of the DNA double helix.[15−17] Indeed, high-resolution X-ray diffraction experiments[16,18−21] and molecular dynamics simulations[22−31] of short B-DNA segments revealed ions localized to the grooves of the helix. From these structures, one can draw several general conclusions about the nature of cation−DNA interactions and competition of cations for binding sites at the DNA surface.

Received: July 3, 2012
Revised: September 26, 2012

   dx.doi.org/10.1021/jp306598y | *J. Phys. Chem. B* XXXX, XXX, XXX−XXX

First, cations are found to preferentially bind guanine bases in the major groove and phosphate groups at the DNA backbone. Second, cation binding to DNA is indirect: more often than not cation−DNA interaction is mediated via water molecules from the first solvation shell of the cation. Third, no specific cation-binding sites exist, but cations localize near several competing electronegative sites.[21] Fourth, according to the NMR studies,[32,33] monovalent cations typically favor minor groove binding,[32,33] although K^+ are relatively more abundant in the major groove than Li^+ and Na^+.[21,34]

The existence of the outer layer of the ion atmosphere is apparent based on the electronegative nature of nucleic acids.[2,13] However, a comprehensive picture of the ion atmosphere—including ion distributions in both inner and outer layers—had remained elusive because of the amorphous and mobile nature of the outer layer. Only recently, advances in anomalous small-angle X-ray scattering (ASAXS) enabled researchers to reveal several general features of the entire ion atmosphere.[13,35−37] First, the ASAXS measurements confirmed that the number of monovalent cations required to neutralize a certain fragment of dsDNA is twice the number of divalent cations required to do the same. Second, the ion atmosphere of divalent cations is more compact than that of monovalent cations, indicating higher binding affinity and greater screening ability of divalent cations. However, despite the tremendous utility of the ASAXS method, it has its limitations.[4] Data obtained using ASAXS are rather qualitative, and many biologically relevant cations (e.g., Na^+, K^+, and Mg^{2+}) are undetectable using this method because of the relatively low electron density of such cations.

Using a novel experimental approach—buffer exchange-atomic emission spectroscopy (BE-AES)[4]—Bai and co-workers were able to explicitly count the number of ions in the atmosphere of a short segment of DNA duplex or triplex (24 or 44 base pairs) for a mixture of two competing cation species and one anion species. Even though these data are more comprehensive and quantitative than the data from ASAXS, the information about spatial distributions and dynamics of the ions is still lacking. With respect to all-atom molecular dynamics (MD) simulations, the BE-AES data is a straightforward benchmark for assessment and refinement of the simulation model. Given a favorable outcome of such an assessment, the simulations can provide the most detailed view of the structure and dynamics of the ion atmosphere.

In this report, we test the ability of all-atom MD simulations to describe the ion atmosphere around a DNA duplex by carrying out a set of simulations that directly match conditions used in the BE-AES experiments. Specifically, we choose the nucleotide sequence of a 24-base pair (bp) DNA duplex and the concentrations of Li^+, Na^+, K^+, and Mg^{2+} cations to be the same as in the BE-AES experiments. Our simulations employ improved parametrization of cation−phosphate interactions,[38] as the standard force fields significantly overestimate the associated attractive force.[38] We find the results of our simulations to be in agreement with the ion-count experimental data, revealing atomically precise spatial distributions of ions and their dynamics in both inner and outer layers of the ion atmosphere.

SIMULATION METHODS

Simulation Setup. To enable direct comparison with experimental ion-counting data,[4] we simulated a 24-bp DNA duplex at various ionic conditions and computed the number of ions around the duplex. The sequence of the DNA duplex was 5′-GGTGACGAGTGAGCTACTGGGCGG-3′, the same as in the experiment. The 5′ and 3′ ends of each DNA strand were terminated with hydroxyl groups using the 5TER and 3TER patches of the CHARMM force field. The net charge of the DNA duplex was −46 e, where e is the charge of a proton.

To realize a dilute DNA condition and minimize potential finite-size artifacts, we employed a relatively large system, measuring approximately 15 nm × 15 nm × 9 nm and consisting of ∼186 000 atoms. Figure 1 illustrates a typical configuration of our simulation system.

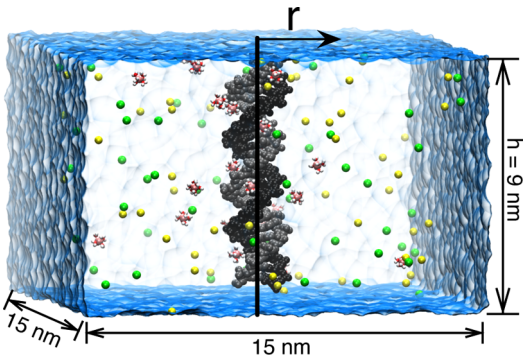

Figure 1. A typical simulation system used in this study. The snapshot features a 24-bp DNA duplex (black or gray), background Na^+ and competing Mg^{2+} cations (BC and CC) and Cl^- anions, shown as yellow, green, and pink spheres, respectively. The hydration shell of Mg^{2+} is shown using the molecular bond representation. The semitransparent surface depicts the simulation volume containing about 186 000 atoms. In all simulations, the axis of the DNA duplex (shown as a black line) is kept parallel to the z-axis using harmonic constraints (eq 1). r is a radial distance from the DNA axis, and h is the dimension of the simulation system in the direction of the DNA axis.

In all simulations, the DNA axis was kept parallel to the z-axis by applying, within the xy-plane, the following harmonic potential to the centers of mass of the upper and lower halves of the molecule:

$$V = 0.5k\{(x_u - x_l)^2 + (y_u - y_l)^2\} \quad (1)$$

where x_u, y_u, x_l, and y_l are the x- and y-coordinates of the centers of mass of the upper (u) and lower (l) halves of dsDNA and k = 1000 kJ/mol·nm^2. This particular setup was chosen to obtain ion concentration profiles up to ∼7 nm away from the DNA helix while minimizing the required computational resources. If DNA were allowed to rotate freely, the simulations would require a significantly larger unit cell to ensure that, for any possible DNA orientation, the interaxial distance between DNA molecules from neighboring images of a unit cell is at least 14 nm. By enforcing DNA to orient along the z axis, we could reduce the system's dimensions along that axis. We chose not to use an effectively infinite DNA model[39] to avoid possible distortions of the DNA structure, as the exact number of DNA base pairs per turn is not an integer number for the DNA sequence of interest. Note that no absolute restraints were applied and, hence, the DNA was allowed to drift about the simulation box.

Ion Counting Protocol. Using the buffer exchange method, Bai et al. explicitly measured the excess number (defined below) of two competing cation species and one anion species when the concentration of one cation remained

dx.doi.org/10.1021/jp306598y | J. Phys. Chem. B XXXX, XXX, XXX−XXX

constant (background cation, BC) and the concentration of the other cation varied (competing cation, CC). Our simulations focus on the three sets of experimental data: CC Li^+, BC Na^+ at 50 mM; CC K^+, BC Na^+ at 50 mM; and CC Na^+, BC Mg^{2+} at 5 mM. In the corresponding experiment, the authors substituted a primary anion Cl^- with cacodylate ion $(AsO_2(CH_3)^{-2})$ because Cl^- was undetectable using their spectrometer.[4] This substitution is not expected to have a considerable effect on the ion counting data.[4] In our simulations, we used Cl^- as the anion species.

To make an ionic solution of specified CC and BC concentrations, we first used the experimental data to estimate the number of ions in the simulation system corresponding to the target BC and CC concentrations. This initial system was equilibrated for >10 ns, yielding the concentration profiles for each ion species $c(r)$ as a function of the distance from the DNA axis, r (e.g., Figure 2A–C). If the bulk concentration of BC (plateau of $c(r)$ at r > 20 Å) deviated from the target value (50 mM for Na^+ and 5 mM for Mg^{2+}), we adjusted the number of BC ions in the simulation and repeated the procedure. When the bulk concentration of BC was within 5 mM of the desired value, the simulation was extended, in most cases, to over 100 ns. Table 1 lists all final production simulations.

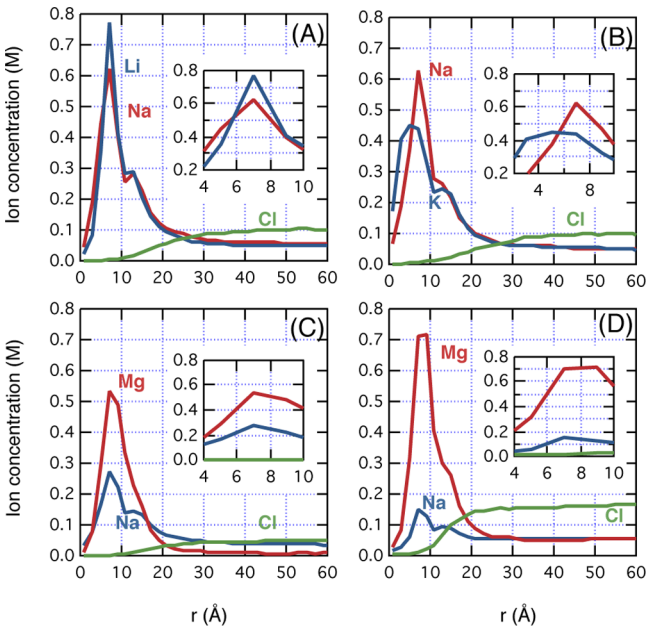

Figure 2. Radial profile of ion concentration, $c(r)$, as a function of the distance from the DNA axis, r, in the simulations of Na50–Li50 (A), Na50–K50 (B), Mg5–Na40 (C), and Mg50–Na50 (D). Insets show a close-up view of the dependences to clarify the location of the concentration maxima.

From a production simulation, the excess number of ions of type i, N_i, was computed by integrating the excess ion concentration, $c_i(r) - c_i(r_{max})$:

$$N_i(r) = \int_0^r \{c_i(r') - c_i(r_{max})\} 2\pi h r' dr' \quad (2)$$

where h is the dimension of the simulation system in the direction of the DNA axis (Figure 1). To compute $c(r)$, we divided the volume around DNA into cylindrical shells $(r, r + \Delta r)$ with r ranging from 0 to r_{max} of 70 Å in Δr = 2 Å increments. The number of ions in each shell was averaged over all frames of the corresponding MD trajectory and divided by the volume of the cylindrical shell, $2\pi r h \Delta r$. Usually, $c_i(r)$ converges to the bulk concentration at r > 40–50 Å. The total charge of ions inside a cylinder of radius r, $Q_{total}(r)$, can be obtained as a linear sum of $N_i(r)$ weighted by valence, z_i:

$$Q_{total}(r) = \sum_i^{ions} z_i N_i(r) \quad (3)$$

Please note that N_i specifies the excess number of ions, which is positive when the ion concentration exceeds the bulk value or negative when the ion concentration is less than the bulk value. One should not confuse N_i with the absolute number of ions. To compute the total charge, one needs to add up the excess number of ions over all ionic species taking into account the absolute value of each ion's charge. At large r, $Q_{total}(r)$ converges to 46 e so that the net charge of DNA (−46 e) is completely neutralized. The effective size of the ion atmosphere can be estimated as the distance at which charge neutralization occurs.

General MD Methods. In our simulations, we used the CHARMM force field for both DNA[40] and ions[41] except for the systems containing Li^+, in which we combined the ion parameters for Li^+, Na^+, and Cl^- from Joung and Cheatham[42] with the CHARMM parameters for nucleic acids. All simulations were performed using our custom NBFIX corrections to nonbounded interaction between cations and phosphate oxygens (or chloride), as described in our recent study.[38]

All MD simulations were carried out using the Gromacs 4.5.1 package[43] with a 2 fs integration time step. The temperature was maintained at 298 K using the Nosé–Hoover scheme.[44,45] The pressure was kept constant at 1 bar using the Parrinello–Rahman scheme.[46] We used a 7–10 Å switching scheme to evaluate van der Waals forces and particle-mesh Ewald (PME) summation[47] to evaluate long-range electrostatic forces. Our PME scheme employed a 1.5 Å grid spacing and a 14 Å cutoff for the real-space Coulomb interaction. SETTLE[48] and LINCS[49] algorithms were used to constrain covalent bonds to hydrogen in water and DNA, respectively. Atom coordinates were recorded every 2 ps.

RESULTS AND DISCUSSION

Following the experimental procedure reported in ref 4, we performed MD simulations of a 24-bp DNA duplex for the following mixtures of cations: Li^+ and Na^+, K^+ and Na^+, and Na^+ and Mg^{2+}. Specifically, we examined several concentrations of Li^+ or K^+ combined with 50 mM Na^+ and several concentrations of Na^+ combined with 5 or 50 mM Mg^{2+}. Throughout this report, cations whose concentration was varied are referred to as competing cations (CC) and cations whose concentration was kept constant are referred to as background cations (BC). Hereafter, [X] denotes the concentration of species X.

The Inner Layer of the Ion Atmosphere. To describe the overall shape of the ion atmosphere around a DNA duplex, we plot, in Figure 2A–D, representative radial profiles of ion concentrations $c(r)$. For better comparison, systems having comparable amounts of CC and BC were chosen: Na50–Li50, Na50–K50, and Mg5–Na40; see Figure 2A–C. Figure 2D presents data for the Mg50–Na50 system, which can be directly compared to the Na50–Li50 and Na50–K50 systems that feature the same 50 mM bulk concentration of Na^+. See

dx.doi.org/10.1021/jp306598y | J. Phys. Chem. B XXXX, XXX, XXX–XXX

Table 1. Summary of All Production Simulations[a]

ion constituents				ion numbers			bulk ion conc. (mM)			
BC	CC	anion	system	BC	CC	Cl^-	[BC]	[CC]	$[Cl^-]$	simul. time (ns)
Na^+	Li^+	Cl^-	Na50−Li50	80	70	104	56	48	102	127
			Na50−Li110	70	150	174	53	115	168	127
			Na50−Li200	63	244	261	51	200	251	120
			Na50−Li430	60	500	514	53	432	485	150
Na^+	K^+	Cl^-	Na50−K50	74	70	104	49	49	98	116
			Na50−K200	63	244	261	50	198	248	157
			Na50−K430	60	500	514	52	433	485	156
Mg^{2+}	Na^+	Cl^-	Mg5−Na20	25	25	29	7	18	28	116
			Mg5−Na40	25	50	54	8	36	51	113
			Mg5−Na70	17	100	88	8	72	84	96
			Mg5−Na240	9	300	272	6	237	250	68
			Mg5−Na420	9	500	472	7	418	431	84
			Mg50−Na50	80	65	179	54	57	167	50

[a]For each system, the table specifies the concentration of ion constituents, the number of ions in the simulation system, ion concentrations away from DNA (bulk concentration), and the total simulation time. Each simulation is abbreviated using the names of the background and competing cations (BC and CC) and their approximate bulk concentrations in equilibrium.

Figures S1−S3 in the Supporting Information for the complete set of ion concentration profiles.

All ion concentration profiles plotted in Figure 2 reach bulk values for r between 30 and 50 Å. The plateaus at large values of r suggest that the simulations reached equilibrium. Figure S4 (Supporting Information) shows the behavior of $c(r)$ for the Na50−Li50 and Mg5−Na40 systems as a function of simulation time. The concentration profiles show no appreciable change as the simulations exceed ∼90 ns.

In the inner layer of the ion atmosphere (r < 15 Å), where ions make direct contact with DNA, the concentration of cations is significantly enhanced, whereas anions are almost completely excluded (Figure 2). In the case when Mg^{2+} competes with Na^+, the concentration of Mg^{2+} near DNA is significantly higher than that of Na^+. For the system shown in Figure 2C, $[Mg^{2+}]$ is about twice $[Na^+]$ for r < 15 Å, whereas bulk $[Na^+]$ is about 5 times that of bulk $[Mg^{2+}]$. When bulk concentrations of Mg^{2+} and Na^+ are comparable, Mg^{2+} dominates in the r < 20 Å region (Figure 2D).

The insets to Figure 2A−D show the locations of the concentration maxima in the radial concentration profiles of cations. For Li^+, Na^+, and Mg^{2+}, the concentration maximum is at r ∼ 7 Å and for K^+ the maximum is at r ∼ 5 Å. As the average distance from the center of the DNA helix to the phosphorus atoms of the DNA backbone is ∼9 Å, the concentration profile plots indicate that some cations localize in the grooves of the DNA. The 2 Å difference in the location of the concentration maximum for K^+ indicates that K^+ binds to the DNA surface at a different location than other cations. Indeed, detailed analysis of the simulation trajectories revealed that K^+ binds more favorably to the major groove, which is deeper than the minor groove (see also Figure 5).

Corresponding to the data shown in Figure 2A−C, we plot the excess number of ions, $N(r)$, in Figure 3A−C for each ion type and the total charge of the ion cloud, $Q_{total}(r)$. Comparison of the total charge plots, Figure 3D, indicates that, regardless of the type and bulk concentration of cations, the total charge of ions located within r < 10 Å is ∼15 e (see also $Q_{total}(r)$ in Figure 3A−C), which amounts to about 30% of the charge of the entire ion atmosphere (46 e). This number is in excellent agreement with measurements of the electrophoretic force on DNA in a nanopore[50] and is consistent with our previous studies of the KCl system.[51] Thus, we conclude that binding of a cation to the grooves is energetically favorable so that, even at low ionic strength, a significant number of cations occupy the grooves. However, the amount of positive charge that can be introduced into the grooves is limited by the finite volume of the grooves and steric and electrostatic repulsion between cations.

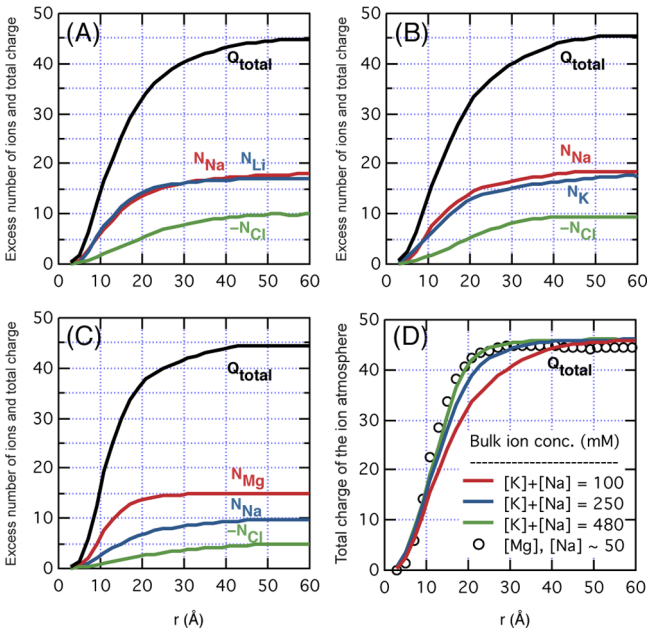

Figure 3. (A−C) The excess numbers of ions, $N_i(r)$, and total charge of the ion atmosphere, $Q_{total}(r)$, in the simulations of Na50−Li50 (A), Na50−K50 (B), and Mg5−Na40 (C) systems. In our systems, $N_i(r)$ is positive for cations and negative for anions, indicating association with and exclusion from the DNA duplex, respectively. (D) Total charge of the ion atmosphere, $Q_{total}(r)$, for the Na50−K50 (red), Na50−K200 (blue), Na50−K430 (green), and Mg50−Na50 (black) systems. The effective size of the ion atmosphere depends on both the overall bulk concentration of cations and the presence of Mg^{2+}.

The Outer Layer of the Ion Atmosphere. In the outer layer of the ion atmosphere, the radial profiles of cation concentration drop rapidly as r exceeds 10 Å. Overall, $c(r)$ exhibits similar decay for all monovalent cations; see Figure

dx.doi.org/10.1021/jp306598y | J. Phys. Chem. B XXXX, XXX, XXX−XXX

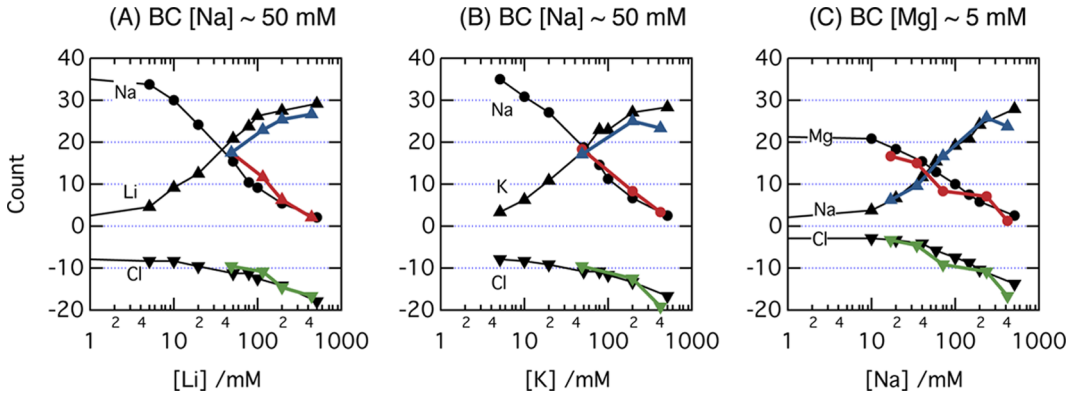

Figure 4. Comparisons between simulated and experimentally measured[4] number of excess ions in ion atmosphere of a DNA duplex. Li^+ (CC) or K^+ (CC) were titrated into a background of 50 mM Na^+ (BC) in parts A and B, respectively. In part C, Na^+ (CC) was titrated into a background of 5 mM Mg^{2+} (BC). In all panels, ●, ▲, and ▼ denote the ion counts for BC, CC, and anion. The simulated ion counts are colored in red (BC), blue (CC), and green (anion). All experimental results are shown in black.

2A,B. The excess number of ions $N(r)$ and the total charge of the ion atmosphere $Q_{total}(r)$ appear to be independent of the type of monovalent cations for r > 10 Å (Figure 3A,B). Such similar behaviors at large distances suggest that ion-specific binding of monovalent cations to DNA[4] occurs not because of the diffuse ion atmosphere at large r but because of direct ion−DNA interactions at small r, in which both structural and chemical characters of DNA play an important role.[11] For Mg^{2+}, the radial concentration profile decays faster than for any monovalent cation (Figure 2C). The plots of the excess number of ions, Figure 3, demonstrate stronger binding of Mg^{2+} to DNA, compared to monovalent cations, which results in a more compact ion atmosphere. For example, $N_{Mg^{2+}}(r)$ converges to a constant value at a smaller distance than $N_{Na^+}(r)$ (Figure 3C).

To quantitatively assess the dependence of the effective size of the ion atmosphere on ion concentration, we plotted the total ion charge, $Q_{total}(r)$, for the Na50−K50, Na50−K200, and Na50−K430 systems in Figure 3D. The comparison clearly shows that the effective size of the ion atmosphere monotonically decreases as the bulk cation concentration increases; e.g., complete charge neutralization is achieved at about r = 30 and 50 Å at a bulk cation concentration of 100 and 480 mM, respectively.

To assess the effect of cation valence on the effective size of the ion atmosphere, we compare the total ion charge, $Q_{total}(r)$, of the Mg50−Na50 system with that of the Na50−K50, Na50−K200, and Na50−K430 systems in Figure 3D. The ion atmosphere of the Na50−K50 system at bulk cation concentration ($[Na^+] + [K^+]$) of 100 mM is larger by 10−20 Å than that of the Mg50−Na50 system, although the latter has comparable bulk cation concentration (or bulk cation charge density of 150 mM). Moreover, the effective size of the ion atmosphere of the Mg50−Na50 system is comparable to that of the Na50−K430 system, although the latter has about 3-fold higher bulk cation charge density. These examples clearly show that the ion atmosphere in the presence of Mg^{2+} is significantly more compact than the ion atmosphere when only monovalent cations are present. Our findings are consistent with the results of the ASAXS measurements[35,36] that predicted reduction of the ion atmosphere in the presence of Mg^{2+}.

Comparison with Experiment. Figure 4 plots the number of excess ions in the atmosphere of a DNA duplex, $N(r \to \infty)$, obtained from experiment[4] and from our MD simulations. Overall, the simulated numbers of excess ions agree well with the data from experiment: the simulated and experimental ion numbers deviate by at most two or three ions. However, among the three data sets, the number of Li^+ is systematically underestimated by about 2 to 3 (Figure 4A). As will be shown below, the simulated binding of Li^+ to all electronegative sites on DNA is comparable to that of Na^+, whereas Bai et al. predicted that Li^+ binds to DNA considerably stronger than Na^+ does. This slight discrepancy indicates that our parametrization of Li^+ has room for improvement, although it is unclear if our parameters underestimate Li^+ affinity to a specific binding site at the surface of DNA or if binding of Li^+ to all electronegative sites is equally underestimated.

For comparison, Figure S5 (Supporting Information) shows the number of excess ions obtained using standard parametrization of cation−phosphate interactions.[41,42] The setup and duration of such simulations were identical to those reported in Figure 4. We found considerable deviations from experiment for systems containing Li^+ (Figure S5A, Supporting Information), as Li^+ binds too strongly to DNA phosphate groups when no NBFIX corrections are applied.[38,52] For the K^+ and Na^+ systems, the results of the simulations were found to be in good agreement with experiment for the range of concentrations studied.

Atomic Scale Features of Cation Binding to Grooves of dsDNA. Before discussing atomic details of cation binding to DNA, it is worthwhile to review known general features of cation−dsDNA interactions.[15,16] Compared to monovalent cations, Mg^{2+} has a greater tendency to orient and polarize water molecules in its first solvation shell and resist dehydration. Consequently, Mg^{2+} resolved in high-resolution crystal structures usually appears fully hydrated, i.e., surrounded by six water molecules. Such hexahydrated Mg^{2+} ions are found either in the major groove (mostly in contact with guanine bases) or in the minor groove (e.g., PDB: 1DPN,[18] 1ENN,[19] 1EN3,[20] 1EN9,[20] 3GGB[21]) of duplex DNA. Consistent with these experimental findings, we explicitly model Mg^{2+} to have such hexahydrated form.[38]

Monovalent cations can also partition into either major or minor grooves, depending on the ion type. For example, a high-resolution crystal structure of B-DNA predicted preferential binding of K^+ to the major groove of dsDNA (PDB: 1JGR).[34] On the other hand, NMR studies predicted preferential binding of Na^+ to the minor groove.[32,33] Because Li^+ has a very low

dx.doi.org/10.1021/jp306598y | J. Phys. Chem. B XXXX, XXX, XXX−XXX

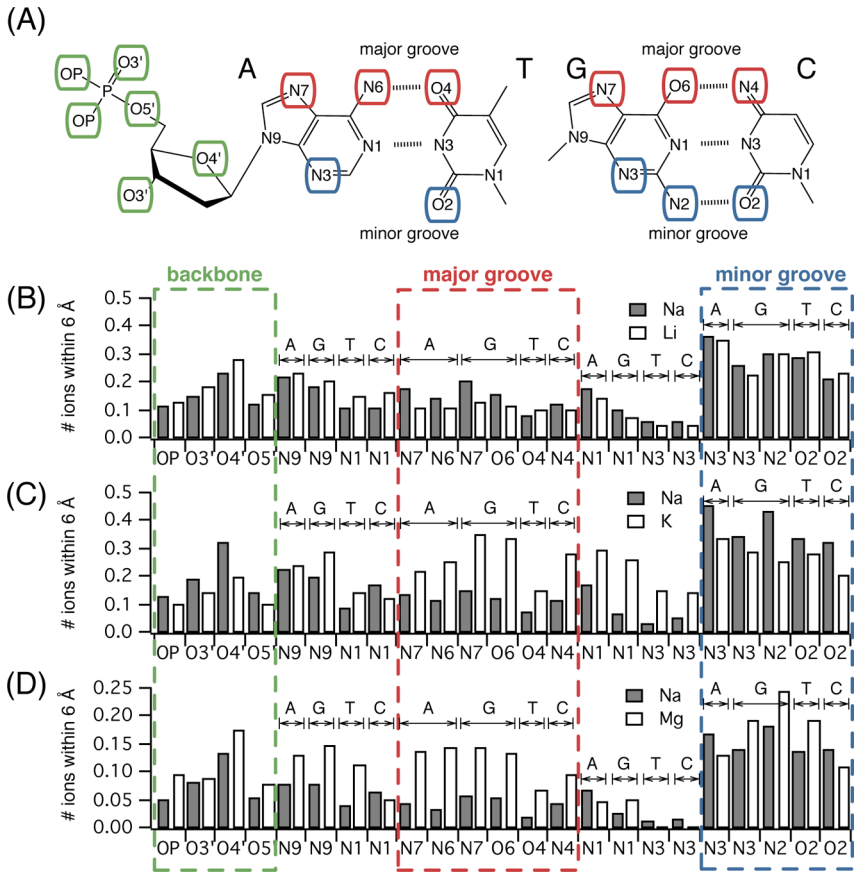

Figure 5. Selective binding of cations to electronegative sites on DNA. (A) Chemical structures of the four DNA nucleotides annotated with the names of the electronegative sites (nitrogen or oxygen). Hydrogens are not shown for clarity. (B, C) The average number of cations (i.e., occupancy) within 6 Å of each electronegative site in the simulations of Na50−Li50 (B), Na50−K50 (C), and Mg5−Na40 (D) systems. The data were obtained by averaging over the entire simulation trajectories.

electron density and is mobile, its binding to dsDNA has not been well characterized by experimental methods. Previous all-atom MD simulations have already shown that K^+ and Na^+ preferentially bind to major and minor dsDNA grooves, respectively.[31] Interestingly, cations localized to phosphate groups are rarely found in crystal structures of B-DNA, despite their large negative charge. The fact that cations can make multiple contacts with several electronegative atoms in the grooves explains why cations prefer the grooves over the phosphate groups. Nevertheless, the phosphate groups make frequent intermittent contact with mobile cations.

To elucidate preferential binding of cations to the surface of DNA, we computed the occupancy of the electronegative atoms by cations in the simulations of Na50−Li50, Na50−K50, and Mg5−Na40 systems.[12] First, we computed the radial distribution functions $g(r)$ of cations around each electronegative atom: $g(r) = \{n(r + \Delta r) - n(r)\}/4\pi\rho\Delta r$, where $n(r)$ is the number of cations of a given type within r from an electronegative atom averaged over the MD trajectory, ρ is the bulk number density of the corresponding cation species, and Δr = 0.1 Å. Figure S8 (Supporting Information) provides examples of $g(r)$ and $n(r)$ for the Na50−Li50 system. The first and second peaks of $g(r)$ are typically located at $r \leq 6$ Å (e.g., Figure S8A, Supporting Information). Hence, we use $n(r = 6$ Å$)$ as a measure of occupancy of the electronegative atom by a species, accounting for direct (first peak in $g(r)$) and solvent mediated (second peak in $g(r)$) contacts. The mean ion occupancy as a function of the atom type and the nucleotide sequence are displayed in Figure 5B−D and Figure S6 (Supporting Information), respectively. Figure 5A displays the chemical structure of the nucleotides annotated with the names of all electronegative atoms.

Figure 5B shows histograms of occupancies of electronegative atoms for competing Na^+ and Li^+ ions at bulk concentrations of 56 and 48 mM, respectively. Overall, the binding sites for Li^+ and Na^+ are very similar, indicating that Li^+ and Na^+ compete for the same binding sites. Both Li^+ and Na^+ prefer the minor groove, although their populations in the major groove are also significant. Occupancy of the backbone O4′ atom is relatively high because a cation can make a simultaneous contact with electronegative atoms in the minor groove and O4′ atom.[53] In the buffer exchange experiment,[4] Li^+ was found to have significantly higher binding affinity to DNA than Na^+. However, Figures 2A, 4A, and 5B indicate that Li^+ binding to DNA is underestimated in our simulations. Although this inconsistency might be caused by imprecise parametrization of Li^+−DNA interactions, it is not clear whether a single specific site or all electronegative sites contribute to this effect.

Figure 5C shows occupancy histograms of electronegative atoms for competing Na^+ and K^+ ions at bulk concentrations of 49 mM, respectively. K^+ is observed to exhibit a considerable preference for the major groove, unlike Li^+ and Na^+. This finding is consistent with experimental studies of thallium (Tl^+), which is an analogue of K^+ because of its similar electronic structure. Crystallographically resolved Tl^+ ions were found near the N7 atoms of two stacked guanines (GpG) or

dx.doi.org/10.1021/jp306598y | J. Phys. Chem. B XXXX, XXX, XXX−XXX

O6 atoms of GpC steps (PDB: 1JGR).[34] Such preferential binding of Tl^+ (or K^+) is consistent with the high K^+ occupancy of the guanine N7 and O6 atoms observed in our simulations (Figure 5C). Figure S6B (Supporting Information) also indicates high populations of K^+ near GpG and GpC steps in the major groove. In the nucleotide sequence used in this study, adenine is surrounded by neighboring guanines, which explains the relatively high K^+ occupancy of the adenine N7 and N6 atoms (Figure 5C). Our results are in qualitative agreement with earlier all-atom MD simulations[31] that found Na^+ and K^+ ions to partition into the minor and major grooves, respectively.

Figure 5D shows occupancy histograms of electronegative atoms for competing Na^+ and Mg^{2+} ions at bulk concentrations of 36 and 8 mM, respectively. Compared with Na^+, Mg^{2+} binds considerably more strongly to the major groove, similar to K^+. Considering the 5-fold difference in the bulk concentrations, the relatively high occupancy of all electronegative atoms by Mg^{2+} clearly indicates greater binding affinity of Mg^{2+} to DNA in comparison with Na^+.

To assess the relative binding affinities of Mg^{2+} and Na^+, we computed the time intervals that Mg^{2+} and Na^+ reside within 6 Å of N3, N7, and OP atoms of DNA from the simulation of the Mg5−Na40 system. These three atoms were chosen to represent binding sites in the minor groove, in the major groove, and at the backbone, respectively. The time interval τ that a cation of a given type resides within 6 Å of a given DNA atom was assigned to one of the eight time-interval groups $\{\tau_g(i)|i = 1, ..., N_g\}$, where $g(=1, ..., 8)$ indicates a particular group (see Figure 6) and N_g is the number of time intervals in

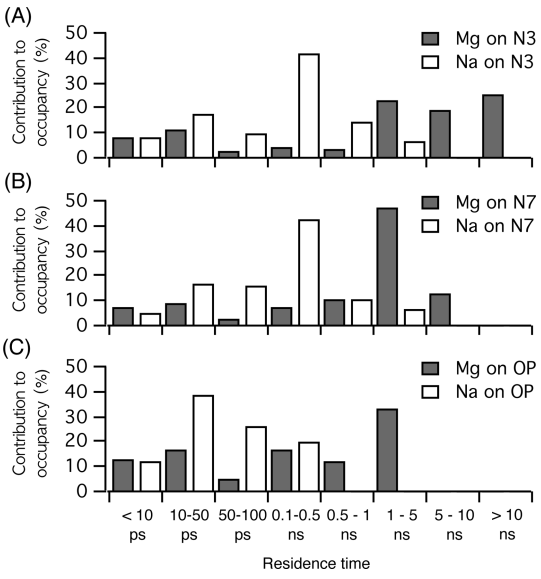

Figure 6. Contribution to DNA atoms' occupancies by contacts from a specific range of ion residence time. Each panel displays data for Mg^{2+} and Na^+ binding in the Mg5−Na40 system for minor-groove atom N3 of purine (A), major-groove atom N7 of purine (B), and backbone atom OP (C).

group g (obtained after analysis of the entire simulation trajectory). The cumulative residence time $\tau_{total} = \sum_g \sum_i \tau_g(i)$ divided by the total simulation time gives the occupancy plotted in Figure 5. In Figure 6, we characterize the distributions of the duration of the specific DNA−cation bonds by plotting the contribution to the occupancy $\sum_i \tau_g(i)/\tau_{total}$ made by bonds from a specific time-interval group g. For all three atoms, the residence time of Mg^{2+} is considerably greater than that of Na^+, confirming that Mg^{2+} binds DNA more strongly than Na^+ does. In the case of Mg^{2+}, long-lived contacts (>1 ns) contribute more than half of the cumulative residence time, whereas short-lived contacts (10−500 ps) account for most of the cumulative residence time for Na^+. In contrast, we found that the distribution of residence times depends to a smaller degree on the type of monovalent cations. In the case of monovalent cations, short-lived contacts (10−500 ps) contribute a major fraction of the cumulative residence time, regardless of the ion type and for all electronegative atoms; see Figure S7 (Supporting Information). The occupancy and residence time of monovalent cations qualitatively agree with the recent report by Kowalczyk et al.,[52] which was performed using our NBFIX corrections, although direct quantitative comparison is difficult due to significant differences in the DNA sequence and ion concentration, and the presence of two cation species.

Figure 7 illustrates the locations of Mg^{2+} and Na^+ binding sites at the surface of dsDNA. Consistent with Figure 5D, Mg^{2+}

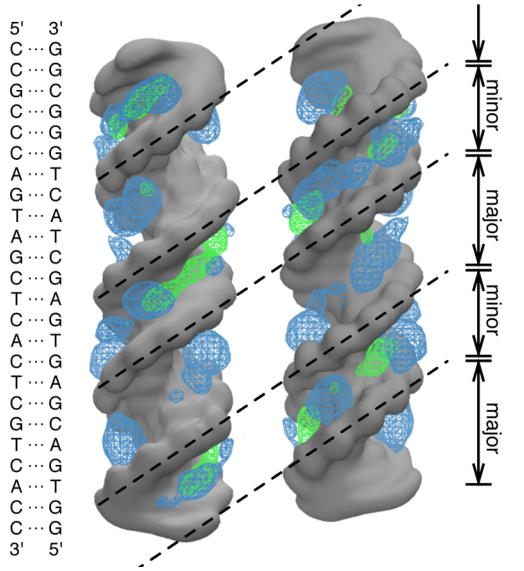

Figure 7. Binding of Mg^{2+} and Na^+ to the grooves of a DNA duplex in the Mg5−Na40 system. Density maps of DNA, Mg^{2+}, and Na^+ were obtained from an ∼100 ns trajectory. The left and right panels show the view of the same DNA molecules from opposite sides. The DNA duplex (gray), Mg^{2+} (blue), and Na^+ (green) are shown as isosurfaces of 0.5 and 0.02 $Å^{-3}$ atom number density for DNA and ions, respectively. The maps were made using the Volmap plugin of VMD.[54]

ions are found in both grooves, while Na^+ mainly occupies the minor groove. Even for monovalent cations that have relatively weakly bound first solvation shells, direct binding to electronegative atoms was rarely observed. Instead, water molecules from the first solvation shell form multiple, simultaneous hydrogen bonds with several electronegative atoms, resulting in a cation density map centered in the middle of the minor groove.[16] In the major groove, the cation density maps are slightly shifted from the geometrical center of the groove, because water from the first solvation shell of the cations cannot form simultaneous contacts with both sides of the major groove.

In Figure 7, the density maps of both Mg^{2+} and Na^+ are broadly distributed along the grooves, suggesting that no specific cation-binding sites exist in either of the grooves.[21]

dx.doi.org/10.1021/jp306598y | J. Phys. Chem. B XXXX, XXX, XXX−XXX

Approximately 4 to 6 cation density peaks can be identified per turn of the DNA helix (20 nucleotides), consistent with our assessment that the total charge of cations buried in the DNA grooves compensates for about 30% of the total DNA charge (Figure 3D) regardless of the composition and concentrations of the cations. The majority of excess cations, which compensate for the remaining 70% of the total DNA charge, stay outside the grooves and interact with the DNA backbone intermittently. We have previously shown that such interactions are short-lived (10−50 ps).[52] Accordingly, we found such short-lived contacts to give major contributions to ion occupancy of the DNA backbone (Figure 6C).

CONCLUDING REMARKS

In this report, we presented the results of all-atom MD simulations that complement experimental characterization of the ion atmosphere around double-stranded DNA.[4] We found that our latest refinement of the all-atom model adequately describes both the inner and outer ionic atmosphere around a DNA duplex, even when two cation species compete to compensate for the DNA charge. In addition to reproducing experimental data, our simulations provided a detailed microscopic account of cation interaction with DNA that is inaccessible to experiment and essential to understanding cation-mediated inter-DNA interactions.[55,56]

Our simulations elucidated general features of the ion atmosphere. In the case when Mg^{2+} competes with Na^+, we found the concentration of Mg^{2+} near DNA to be considerably greater than that of Na^+. Whereas the absolute and relative concentrations of different cation species inside DNA ($r < 10$ Å) vary depending on the properties of the bulk solution, cations buried in the grooves amount to a charge that can compensate for about 30% of the total DNA charge. The effective size of the ion atmosphere was found to decrease with increasing cation concentration and/or valence.

Our simulations provided detailed information about preferential binding of cations to electronegative atoms at the surface of DNA. We found that Li^+ and Na^+ preferentially bind to the minor groove of a DNA duplex. On the other hand, K^+ and Mg^{2+} were found to bind the major groove significantly more than Li^+ and Na^+ do. Consistent with the high-resolution crystallographic structure, we observed enhanced populations of cations near guanine bases in the major groove. Nevertheless, we were unable to find general rules for sequence-specific binding of cations, in part because we considered only one (heterogeneous) sequence in this study. In general, we did not observe permanent and cation-specific binding sites at the surface of DNA. Instead, cations were observed to make simultaneous contacts with multiple competing electronegative sites. In the case of Mg^{2+}, the majority of the contacts lasted more than 1 ns, whereas, in the case of Li^+, Na^+, and K^+, most of the contacts were within the 10−500 ps range.

ASSOCIATED CONTENT

Supporting Information

Radial profiles of ion concentration, number of excess ions obtained in simulations performed without using NBFIX corrections, mean occupancy of electronegative atoms of each DNA base pair by ions, contribution to occupancies by contacts from a specific range of ion residence time, and exemplary radial distribution functions of ions. This material is available free of charge via the Internet at http://pubs.acs.org.

AUTHOR INFORMATION

Corresponding Author

*E-mail: aksiment@illinois.edu.

Notes

The authors declare no competing financial interest.

ACKNOWLEDGMENTS

This work was supported by the Center for the Physics of Living Cells through a grant from the National Science Foundation (PHY0822613). Supercomputer time was provided at XSEDE via XSEDE Resources Allocation Grant MCA05S028 and the Taub cluster (UIUC). A.A. would like to thank the Department of Bionanosciences at Delft University for hospitality and support from The Netherlands Organisation for Scientific Research (NWO).

REFERENCES

(1) Alberts, B.; Johnson, A.; Lewis, J.; Raff, M.; Roberts, K.; Walter, P. *Molecular Biology of The Cell*, 5th ed.; Garland Science: New York, London, 2007.
(2) Manning, G. S. *J. Chem. Phys.* **1969**, *51*, 924.
(3) Draper, D.; Grilley, D.; Soto, A. *Annu. Rev. Biophys. Biomol. Struct.* **2005**, *34*, 221−243.
(4) Bai, Y.; Greenfeld, M.; Travers, K.; Chu, V.; Lipfert, J.; Doniach, S.; Herschlag, D. *J. Am. Chem. Soc.* **2007**, *129*, 14981−14988.
(5) Rau, D. C.; Lee, B.; Parsegian, V. A. *Proc. Natl. Acad. Sci. U.S.A.* **1984**, *81*, 2621−2625.
(6) Knobler, C.; Gelbart, W. *Annu. Rev. Phys. Chem.* **2009**, *60*, 367−383.
(7) Koculi, E.; Hyeon, C.; Thirumalai, D.; Woodson, S. A. *J. Am. Chem. Soc.* **2007**, *129*, 2676−2682.
(8) Li, P.; Vieregg, J.; Tinoco, I. *Annu. Rev. Biochem.* **2008**, *77*, 77−100.
(9) Fedor, M. *Annu. Rev. Biophys.* **2009**, *38*, 271−299.
(10) MacKerell, A., Jr.; Nilsson, L. *Curr. Opin. Struct. Biol.* **2008**, *18*, 194−199.
(11) Chu, V. B.; Bai, Y.; Lipfert, J.; Herschlag, D.; Doniach, S. *Biophys. J.* **2007**, *93*, 3202−3209.
(12) Kirmizialtin, S.; Elber, R. *J. Phys. Chem. B* **2010**, *114*, 8207−8220.
(13) Chu, V.; Bai, Y.; Lipfert, J.; Herschlag, D.; Doniach, S. *Curr. Opin. Chem. Biol.* **2008**, *12*, 619−625.
(14) Bacquet, R. J.; Rossky, P. J. *J. Phys. Chem.* **1988**, *92*, 3604−3612.
(15) Williams, L. D.; Maher, L. J. *Annu. Rev. Biophys. Biomol. Struct.* **2000**, *29*, 497−521.
(16) Subirana, J. A.; Soler-Lopez, M. *Annu. Rev. Biophys. Biomol. Struct.* **2003**, *32*, 27−45.
(17) Pabit, S. A.; Qiu, X.; Lamb, J. S.; Li, L.; Meisburger, S. P.; Pollack, L. *Nucleic Acids Res.* **2009**, *37*, 3887−3896.
(18) Egli, M.; Tereshko, V.; Teplova, M.; Minasov, G.; Joachimiak, A.; Sanishvili, R.; Weeks, C. M.; Miller, R.; Maier, M. A.; An, H.; Dan Cook, P.; Manoharan, M. *Biopolymers* **1998**, *48*, 234−252.
(19) Soler-López, M.; Malinina, L.; Liu, J.; Huynh-Dinh, T.; Subirana, J. A. *J. Biol. Chem.* **1999**, *274*, 23683−23686.
(20) Chiu, T. K.; Dickerson, R. E. *J. Mol. Biol.* **2000**, *301*, 915−945.
(21) Maehigashi, T.; Hsiao, C.; Kruger Woods, K.; Moulaei, T.; Hud, N. V.; Dean Williams, L. *Nucleic Acids Res.* **2011**, *40*, 3714−3722.
(22) Korolev, N.; Lyubartsev, A. P.; Laaksonen, A.; Nordenskiöld, L. *Biophys. J.* **2002**, *82*, 2860−2875.
(23) Auffinger, P.; Westhof, E. *J. Mol. Biol.* **2000**, *300*, 1113−1131.
(24) Auffinger, P.; Westhof, E. *J. Mol. Biol.* **2001**, *305*, 1057−1072.
(25) Jayaram, B.; Beveridge, D. L. *Annu. Rev. Biophys. Biomol. Struct.* **1996**, *25*, 367−394.
(26) Young, M. A.; Jayaram, B.; Beveridge, D. L. *J. Am. Chem. Soc.* **1997**, *119*, 59.
(27) Cheng, Y.; Korolev, N.; Nordenskiàěńld, L. *Nucleic Acids Res.* **2006**, *34*, 686−696.

(28) Ponomarev, S.; Thayer, K. M.; Beveridge, D. L. *Proc. Natl. Acad. Sci. U.S.A.* **2004**, *101*, 14771−14775.
(29) Sen, S.; Andreatta, D.; Ponomarev, S. Y.; Beveridge, D. L.; Berg, M. A. *J. Am. Chem. Soc.* **2009**, *131*, 1724−1735.
(30) Li, W.; Nordenskiöld, L.; Mu, Y. *J. Phys. Chem. B* **2011**, *115*, 14713−14720.
(31) Várnai, P.; Zakrzewska, K. *Nucleic Acids Res.* **2004**, *32*, 4269−4280.
(32) Denisov, V. P.; Halle, B. *Proc. Natl. Acad. Sci. U.S.A.* **2000**, *97*, 629−633.
(33) Cesare Marincola, F.; Denisov, V. P.; Halle, B. *J. Am. Chem. Soc.* **2004**, *126*, 6739−6750.
(34) Howerton, S. B.; Sines, C. C.; VanDerveer, D.; Williams, L. D. *Biochemistry* **2001**, *40*, 10023−10031.
(35) Das, R.; Mills, T. T.; Kwok, L. W.; Maskel, G. S.; Millett, I. S.; Doniach, S.; Finkelstein, K. D.; Herschlag, D.; Pollack, L. *Phys. Rev. Lett.* **2003**, *90*, 188103.
(36) Andresen, K.; Das, R.; Park, H. Y.; Smith, H.; Kwok, L. W.; Lamb, J. S.; Kirkland, E. J.; Herschlag, D.; Finkelstein, K. D.; Pollack, L. *Phys. Rev. Lett.* **2004**, *93*, 248103.
(37) Wong, G. C. L.; Pollack, L. *Annu. Rev. Phys. Chem.* **2010**, *61*, 171−189.
(38) Yoo, J.; Aksimentiev, A. *J. Phys. Chem. Lett.* **2012**, *3*, 45−50.
(39) Luan, B.; Aksimentiev, A. *Phys. Rev. Lett.* **2008**, *101*, 118101.
(40) MacKerell, A., Jr; Banavali, N. *J. Comput. Chem.* **2000**, *21*, 105−120.
(41) Beglov, D.; Roux, B. *J. Chem. Phys.* **1994**, *100*, 9050−9063.
(42) Joung, I. S.; Cheatham, T. E. *J. Phys. Chem. B* **2008**, *112*, 9020−9041.
(43) Hess, B.; Kutzner, C.; Van Der Spoel, D.; Lindahl, E. *J. Chem. Theory Comput.* **2008**, *4*, 435−447.
(44) Nose, S.; Klein, M. L. *Mol. Phys.* **1983**, *50*, 1055−1076.
(45) Hoover, W. G. *Phys. Rev. A* **1985**, *31*, 1695−1697.
(46) Parrinello, M.; Rahman, A. *J. Appl. Phys.* **1981**, *52*, 7182−7190.
(47) Darden, T.; York, D.; Pedersen, L. *J. Chem. Phys.* **1993**, *98*, 10089−10092.
(48) Miyamoto, S.; Kollman, P. A. *J. Comput. Chem.* **1992**, *13*, 952−962.
(49) Hess, B.; Bekker, H.; Berendsen, H. J. C.; Fraaije, J. G. E. M. *J. Comput. Chem.* **1997**, *18*, 1463−1472.
(50) van Dorp, S.; Keyser, U. F.; Dekker, N. H.; Dekker, C.; Lemay, S. G. *Nat. Phys.* **2009**, *5*, 347−351.
(51) Luan, B.; Aksimentiev, A. *Phys. Rev. E* **2008**, *78*, 021912.
(52) Kowalczyk, S. W.; Wells, D. B.; Aksimentiev, A.; Dekker, C. *Nano Lett.* **2012**, *12*, 1038−1044.
(53) Shui, X.; Sines, C. C.; McFail-Isom, L.; VanDerveer, D.; Williams, L. D. *Biochemistry* **1998**, *37*, 16877−16887.
(54) Humphrey, W.; Dalke, A.; Schulten, K. *J. Mol. Graphics* **1996**, *14*, 33−38.
(55) Luan, B.; Aksimentiev, A. *J. Am. Chem. Soc.* **2008**, *130*, 15754−15755.
(56) Maffeo, C.; Schöpflin, R.; Brutzer, H.; Stehr, R.; Aksimentiev, A.; Wedemann, G.; Seidel, R. *Phys. Rev. Lett.* **2010**, *105*, 158101.